Journal of Catalysis **200,** 250–258 (2001)
doi:10.1006/jcat.2001.3213, available online at http://www.idealibrary.com on IDEAL®

Structure and Redox Behavior of Zirconium in Microporous Zr-Silicalites Studied by EXAFS and ESR Techniques

Veda Ramaswamy,* Bhavana Tripathi,* D. Srinivas,* A. V. Ramaswamy,*,[1]
Ricardo Cattaneo,† and Roel Prins†

*Catalysis Division, National Chemical Laboratory, Pune 411 008, India; and †Laboratory of Technical Chemistry, ETH, Zurich, Switzerland

Received September 8, 2000; revised January 5, 2001; accepted January 12, 2001; published online May 15, 2001

The local environment of zirconium in Zr-silicalite with MEL structure has been studied using the EXAFS technique. The structural parameters indicate the presence of tetrahedrally coordinated, isolated zirconium sites with Si–O–Zr linkages. The experimental results support the location of Zr^{4+} ions at edge- or corner-sharing positions (N(Zr–O) = 3.9 and N(Zr–Si) = 1.2), rather than in regular substitutional positions. The isolated Zr^{4+} ions could be reduced to the Zr^{3+} state on treatment with H_2 followed by UV irradiation. The ESR spectra of reduced Zr-silicalite samples of both MFI and MEL structures reveal a distorted tetrahedral geometry around Zr^{3+} and a $d_{x^2-y^2}$ orbital ground state. The ESR results are consistent with EXAFS findings. The role of these active Zr species in the selective oxidation of phenol is investigated by ESR after interaction of the samples with aqueous H_2O_2. The formation of a Zr^{4+}–$O_2^{-\bullet}$ radical species, and the variation in the g parameter under the influence of solvents such as water, acetonitrile, and methanol are reported. The results confirm the role of Zr^{4+} as active centers. The coordination of solvent molecules around Zr centers affects the catalytic activity to different extents, in agreement with the difference in ESR signal intensity of the radical species. These isolated active sites are responsible for the formation of superoxide/hydroperoxide species through which the oxygen is transferred to the substrate in the hydroxylation of phenol.

Key Words: **Zr-silicalites; microporous Zr-silicates; EXAFS; ESR; selective oxidation; hydroxylation of phenol; oxidation with H_2O_2.**

INTRODUCTION

The catalytic applications of microporous metallosilicates have been of wide interest particularly in selective oxidation reactions. For high catalytic activity and selectivity, it is customary to have a sufficient concentration of structurally well defined metal centers accessible in the silicalite framework structure. It is, therefore, critical to prove unequivocally the isomorphous substitution of a transition metal ion in the framework structure of metallosilicates. In this regard, X-ray absorption spectroscopic methods, such as the extended X-ray absorption fine structure (EXAFS) technique, have played an increasingly important role in structural studies. The EXAFS method is particularly useful for investigating the local structure (coordination number, near-neighbor atoms, bond distances) of framework as well as extraframework atoms. For example, unequivocal evidence for the framework substitution of Ti in titanium silicalites with MFI structure (TS-1) has been established by detailed EXAFS studies (1–6). The applicability of *in situ* EXAFS spectroscopy to time-resolved processes in zeolite-based catalysts has been demonstrated by Hatje *et al.* (7). Migration of metal ions from framework to extraframework positions has also been studied by EXAFS on other metal substituted silicalites, e.g., Fe-MFI (8), Ga-MFI (9), and Ga-beta (10).

In earlier reports on zirconium-containing silicalites of MFI (Zr-Sil-1) and MEL (Zr-Sil-2) structures, XRD and other spectroscopic techniques (UV–visible and FT-IR) have been employed to investigate the possibility of substitution of Zr^{4+} ions in framework positions (11, 12). The catalytic activity of Zr-Sil-2 in the hydroxylation of phenol with aqueous H_2O_2 was also reported. The XRD studies have revealed a linear increase in the lattice parameters for the Zr-Sil-2 samples with increasing zirconium content up to one Zr atom per unit cell. This observation suggests that the Zr^{4+} ions could be incorporated in the silicalite framework up to a concentration of one Zr atom per unit cell and that at higher concentrations, extraframework Zr species are formed. The observed higher Lewis acidity in Zr-Sil-2 samples compared to Zr-free silicalite samples in pyridine adsorption studies were correlated to the polar nature of Si–O–Zr linkages compared to the Si–O–Si bonds (12).

In this communication, we report on the local structure of the framework zirconium in the silicalite structure using the EXAFS technique. The reducibility of framework Zr^{4+} with hydrogen followed by UV irradiation, and the intermediate paramagnetic superoxide/hydroperoxide species formed by the interaction with aqueous hydrogen peroxide, are investigated by ESR spectroscopy. Successful incorporation of Zr^{4+} ions is possible at low concentrations (Si/Zr >100) without the formation of Zr–O–Zr linkages, by a careful synthetic procedure (11–14). Eventually, these

[1] To whom correspondence should be addressed. Fax: +91-20-5893761. E-mail: avr@ems.ncl.res.in.

0021-9517/01 $35.00

isolated Zr^{4+} ions are found to be the active centers in the catalytic hydroxylation of phenol.

EXPERIMENTAL

Materials and Synthesis of Zr-Sil-1 and Zr-Sil-2

The hydrothermal syntheses of zirconium-silicates with MFI and MEL structures (Zr-Sil-1 and Zr-Sil-2, respectively) were carried out using the following molar compositions of the gels: 1.0 SiO_2 : x ZrO_2 : 0.5 TPAOH : 30 H_2O and 1.0 SiO_2 : x ZrO_2 : 0.4 TBAOH : 30 H_2O, respectively, where $x = 0.0033$ to 0.02. Other details of the synthesis are given elsewhere (11, 12). For comparison, silica polymorphs of MFI and MEL structures (Sil-1 and Sil-2, respectively) were prepared, impregnated with an aqueous solution of $ZrCl_4$, and then calcined at 773 K in order to get Zr-impregnated Sil-1 and Sil-2, samples, respectively.

Methods

EXAFS studies. The EXAFS spectra were collected at the Swiss Norwegian beamline (BM01) at the European Synchrotron Radiation Facility (ESRF), France. A Si 111 monochromator was used for the EXAFS measurements. The absorption was measured by means of ionization chambers. The beam was unfocused and a gold mirror was used to reject higher harmonic radiation. Prior to these experiments, the samples were pressed into a self-supporting wafer in a special EXAFS cell and treated at 673 K in He flow for 3 h. The samples were left in the cell under a He atmosphere, and cooled to 77 K. During the measurement, three scans were averaged to obtain a good signal-to-noise ratio. The k-range used for the analysis was 3.0–19.0 $Å^{-1}$. For these studies, we selected a sample of Zr-Sil-2 (MEL structure) with an optimum Zr content ($SiO_2/ZrO_2 = 102$), which was studied by other characterization techniques (12). The Zr K-edge EXAFS spectrum of the Zr-Sil-2 sample was compared to that of monoclinic zirconia with sevenfold coordination due to the unavailability of a tetrahedral Zr oxide standard. The spectra were analyzed using the XDAP program (15). The used references were produced by means of feff7 (16). A single scattering approach was employed.

ESR spectroscopy. The ESR spectra were recorded at 298 and 77 K on a Bruker EMX X-band spectrometer with 100 kHz field modulation. The calcined powder samples were placed in Suprasil quartz cells (4.5 mm OD), suitably designed for *in situ* evacuation treatments. Prior to the ESR experiments, the samples were evacuated for 5 h at 673 K, cooled to 298 K, and then flushed with 5% hydrogen in argon gas. The flow of hydrogen was allowed for 15–30 min as pretreatment of the sample. The hydrogen-treated sample was then irradiated by UV radiation for 20 min using a UV lamp (200–290 nm; 400 W) and the ESR spectrum was recorded immediately. With either of the treatments alone the samples did not show any ESR spectra.

In the experiments with aqueous H_2O_2, a freshly calcined sample was interacted with 50% aqueous H_2O_2 at 298 K and then the ESR spectra were recorded. In other experiments, the samples were initially soaked in different solvents (water, methanol, and acetonitrile), the excess of solvent was removed, and the moist solid samples were interacted with H_2O_2 and then the ESR spectra were recorded. The signal-to-noise ratio of the ESR spectra was improved by averaging the results of 10 repeated scans. DPPH was used as a field marker. The microwave frequency was calibrated by a frequency counter built in the ER 041 XG-D microwave bridge. Spectral manipulations and simulations were done using the Bruker WINEPR and Simfonia software packages.

RESULTS AND DISCUSSION

Structure of Zirconium in Zr-Sil-2

The EXAFS data of the Zr-Sil-2 sample are presented in Fig. 1. Trace a of Fig. 1 shows the plot of $k^3\chi(k)$ versus k, wherein k is the photoelectron wave vector and $\chi(k)$ the normalized absorption coefficient. This experimental curve was obtained after elimination of a high-frequency component by Fourier transformation and then fitting of the experimental data. The corresponding Fourier transform of $k^3\chi(k)$ versus R is shown in trace b of Fig. 1. The extraction of the EXAFS function showed a maximum at 1 Å even when the k range of the used $\chi(k)$ data was reduced. The signal cannot be removed without removing important information from the spectrum. The presence of the shoulder does not influence the results significantly. The structural and the least-squares fitting parameters of Zr-Sil-2 obtained by the data analysis along with standard deviations are given in Table 1. The EXAFS results reveal that each Zr atom is linked to four equivalent oxygen atoms ($N = 3.81$), located at an average bond distance of 1.945 Å. The static disorder value, σ^2 (of the order of 10^{-4} $Å^2$), for the distribution of interatomic distances within a given shell reveals an ordered structure in the first coordination shell.

The next neighboring atom could be Si or Zr. However, the observed R value of 3.35 Å is quite different from the Zr–Zr distance of 3.45 Å in monoclinic zirconia and 3.64 Å in tetragonal zirconia (17). This rules out the possibility of adjacent or next-neighbor Zr atoms, and instead, supports the presence of isolated ZrO_4, corner- or edge-shared with a SiO_4 tetrahedron. In agreement with this result, the absorptions due to Zr–O–Zr and Zr=O species were absent in the UV–visible spectra of Zr-silicalite samples (12).

If Zr occupies a regular substitutional location (structure I), the coordination number (N) for the second shell should be 4. However, the value of 1.21 observed in the present case

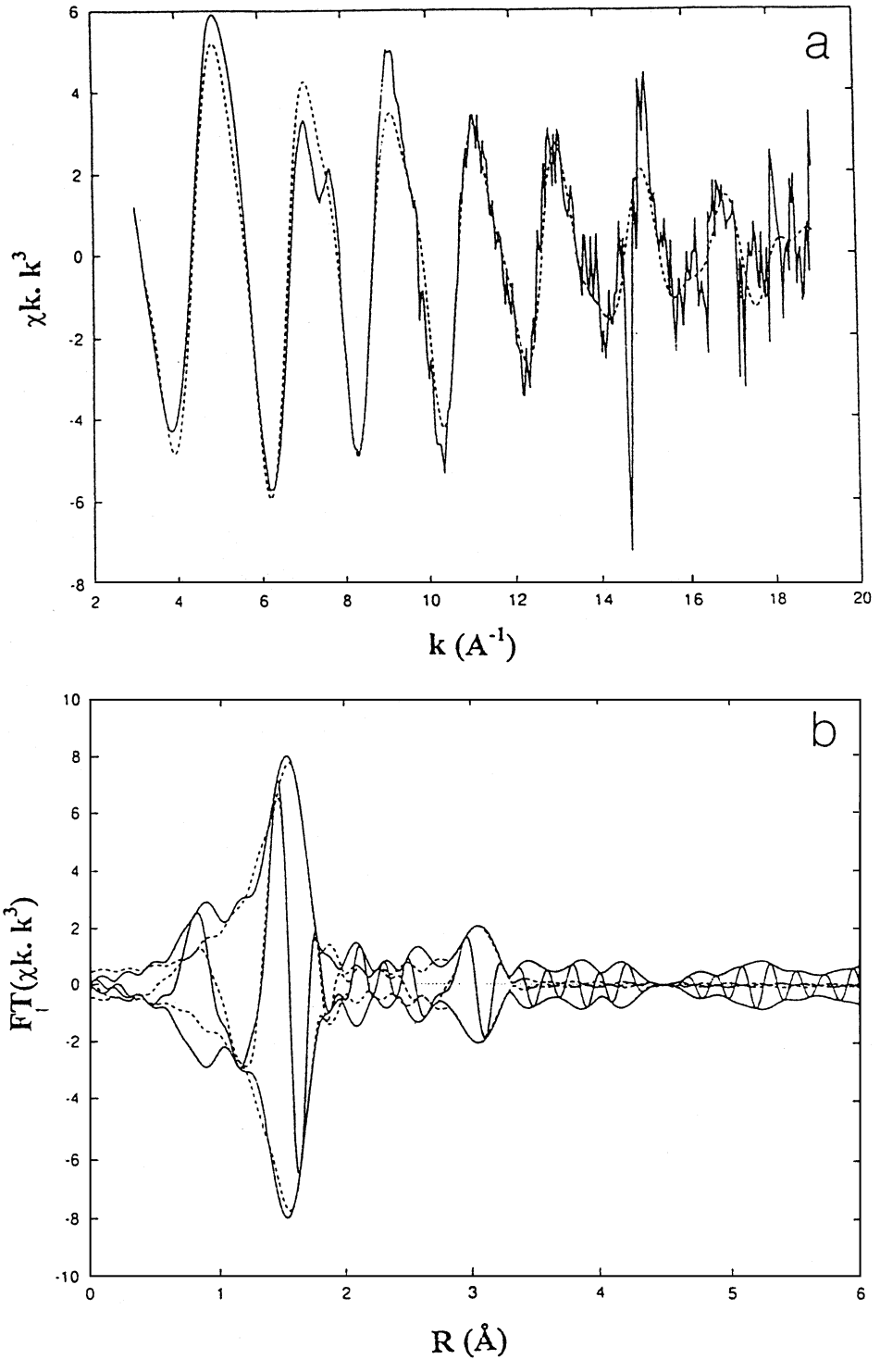

FIG. 1. EXAFS spectra of Zr-Sil-2: (a) the $k^3\chi(k)$ data recorded at the Zr K-edge and (b) Fourier transforms of $k^3\chi(k)$ data versus R (Å). (Experimental, —, and fitted data, $\cdots$).

indicates the possible structures II and III, representing the location of Zr at the corner- or edge-sharing positions. One or two of the oxygen atoms in structure III can correspond to terminal OH groups while the rest belong to the framework structure. The ZrO_4 units are linked through an edge with SiO_4 tetrahedra and are different from the usual isomorphous substitution sites. The distortion and the strain in the zeolite framework are expected to be smaller for an edge-sharing linkage compared to an isomorphous substitutional site.

TABLE 1

EXAFS Structural and Least-Squares Fitting Parameters Obtained for Zr in Zr-Sil-2 Sample[a]

Shell	Back scatterer	N	$\triangle\sigma^2$ (Å^2)	R (Å)	E_0-corr ΔE (eV)
1	Zr-O	3.81 ± 0.25	-0.000974 ± 0.00142	1.945 ± 0.008	5.21 ± 0.74
2	Zr-Si	1.21 ± 0.38	-0.00212 ± 0.00591	3.35 ± 0.042	-12.83 ± 2.09

[a] Least-squares fitting parameters: N = number of atoms coordinated to Zr atom; σ^2 = Debye–Waller factor; R = nearest-neighbor position; E_0 = threshold energy.

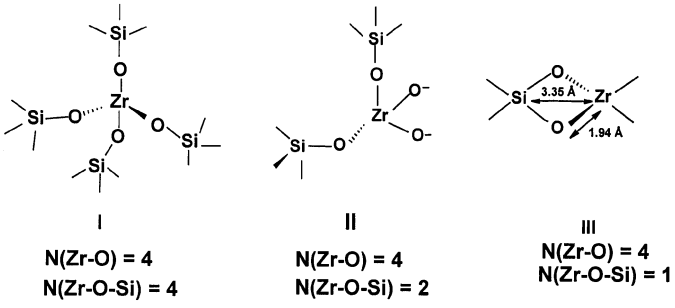

Redox Behavior of Zirconium in Zr-Silicalites

ESR spectroscopy has been used extensively to examine the redox properties of transition metal ions in metallosilicates and metal-supported oxides (18–20). The transition metal ions in the molecular sieves can be reduced by several methods including (a) thermal treatment at higher temperatures, (b) reaction with H_2 or CO at moderate to high temperatures, and (c) UV or γ-ray irradiation. Although the zirconium-containing silicalite samples (Zr-Sil-1 and Zr-Sil-2) are supposed to be diamagnetic, they showed, at 298 K, a weak ESR signal at $g \approx 4.23$ and a broad signal at $g \approx 2.23$ corresponding to an Fe^{3+} impurity. The samples were initially evacuated at 773 K and 0.133 Pa for about 6 h and then exposed to hydrogen at 298 K for 15–30 min. Subsequently, the samples were irradiated with UV light (200–290 nm; 400 W output) for about 20 min and the ESR spectra were recorded at 77 K. The spectra for the reduced samples of Zr-Sil-1 and Zr-Sil-2 were somewhat similar. However, the intensities of the ESR signals were smaller in Zr-Sil-1 than in Zr-Sil-2. A typical spectrum for Zr-Sil-2 at 77 K is shown in Fig. 2a.

The ESR spectrum reveals two types of species: species 1 in Zr-Sil-1 is characterized by signals at $g_x = 1.982$, g_y, $= 1.973$, and $g_z = 1.968$ and in Zr-Sil-2 at $g_x = 1.982$, $g_y = 1.973$, and $g_z = 1.963$; species II is characterized by signals at $g_x = 2.000$, $g_y = 2.008$, and $g_z = 2.033$. The signals for species I below the free-spin g value ($g_e = 2.0023$) correspond to Zr^{3+} ions and those for species II above the free-spin g value are attributed to zirconium superoxide radical anions ($Zr^{4+}(O_2^{-\bullet})$). The signals corresponding to species I and II are marked in Fig. 2a. The rhombic g symmetry for both species I and II indicates that the crystal field symmetry at Zr is as low as C_{2v}. The variation in the g values of species I in Zr-Sil-1 and Zr-Sil-2 reveals subtle differences in the location and local symmetry of Zr^{3+} ions and the crystal field stabilization energy in the two types of samples. Reduction of Zr^{4+} to Zr^{3+} was not observed with either of the treatments (i.e., H_2 at 298 K or UV irradiation) alone. It was also noticed that the intensity of the signals was

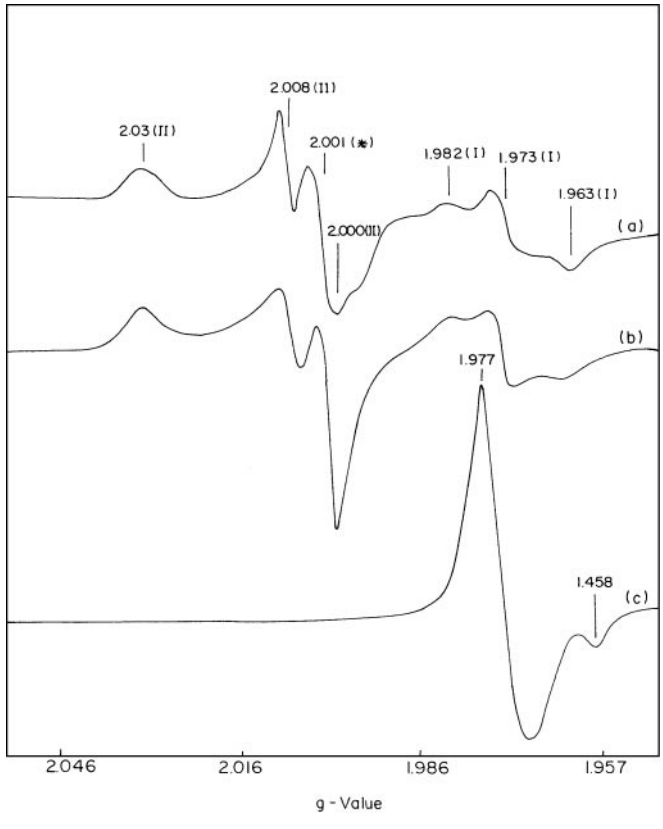

FIG. 2. X-band ESR spectra of (a) Zr-Sil-2 after interacting with H_2 followed by UV irradiation, (b) simulated spectrum of (a), and (c) Zr-impregnated Sil-2 sample after thermal treatment at 1073 K. The g parameters of Zr^{3+} (species I) and Zr ($O_2^{-\bullet}$) (species II) are marked. The unusual line shape is due to overlap of signals and interference with the Fe^{3+} background signal. The signal at $g = 2.001$ denoted by an asterisk corresponds to a free radical, the origin of which is not known.

higher when the irradiation wavelength used was 200 nm compared to 290 nm. The wavelength dependence of ESR signal intensity is perhaps related to the oxygen-to-Zr(IV) charge transfer transition. Neat ZrO_2 exhibits this transition in the UV region around 240 nm. But Zr-silicalites with isolated, tetrahedral zirconium oxide show the charge transfer transition around 212 nm (11). Although we are not very sure at this time about the mechanism of reduction, we strongly believe that it is associated with a ligand-to-metal ($O(2p) \rightarrow Zr(4d)$) charge transfer transition and hydrogen addition. As the reduction is associated with the charge transfer transition, the concentration of Zr^{3+} ions and the ESR signal intensity are dependent on the charge transfer band position (in Zr-Sil samples this transition occurs at 212 nm) and the wavelength of the UV radiation. Quantitative study on the amount of Zr^{3+} ions could not be done. Prolonged irradiation did not increase the ESR signal intensity and perhaps indicates that the majority of zirconium is reduced to the Zr^{3+} state at 298 K on hydrogen treatment followed by UV irradiation. The H_2/UV irradiation treatment reduces most of the Zr^{4+} to Zr^{3+} ions. However, the latter ions were highly reactive toward aerial oxygen and form stable Zr ($O_2^{-\bullet}$) radical anions (species II). Taking a known concentration of superoxide generated by interaction of Zr propoxide with H_2O_2 as standard, we found that 14% of total Zr^{4+} is transformed to Zr($O_2^{-\bullet}$) species in H_2–UV irradiation treatments.

Reduction of Zr^{4+} to Zr^{3+} due to thermal treatment was possible only in Zr-impregnated silicalite samples at 1073 K (Fig. 2b). However, the spectral parameters of the Zr^{3+} ions are different ($g_\perp$ or $g_{x/y} = 1.977$ and $g_\parallel$ or $g_z = 1.958$) from those of Zr-Sil-1 and Zr-Sil-2 reduced by H_2–UV irradiation. It is pertinent to note that the *g* parameters for the Zr-impregnated silicalite samples are in excellent agreement with the values reported by Morterra *et al.* for surface Zr^{3+} ions in activated ZrO_2 ($g_\perp = 1.978$ and $g_\parallel = 1.953$) (21). However, the rhombic symmetry and the difference in *g* values of Zr-Sil-1 and Zr-Sil-2 suggest that Zr ions in these samples are probably located inside the pore structure. The inertness toward thermal treatment and the observed higher intensity of ESR signals after irradiation with higher energy UV radiation suggest that the zirconium ions in the pore structure are more difficult to reduce than the ions at the surface of the silicalite structure.

The energy level orderings of *d* orbitals in tetrahedral and octahedral crystal field environments are shown in Figs. 3a and 3b, respectively. In a tetrahedral crystal field a d^1 ion will have the *E* state lowest. A further tetrahedral distortion will remove the orbital degeneracy of the ground state as shown in Fig. 3a. If the distortion is positive (i.e., tetragonal compression), the $d_{3z^2-r^2}$ state will lie lower. Conversely, if the distortion is negative (i.e., tetragonal elongation), the $d_{x^2-y^2}$ state lies lower. For positive

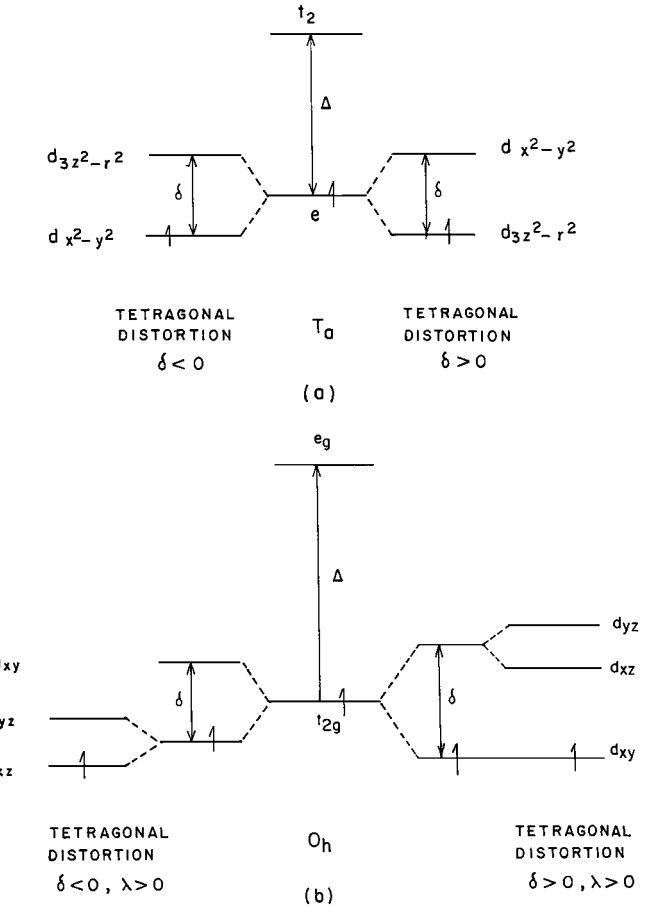

FIG. 3. Energy level ordering of *d*-orbitals in (a) tetrahedral and (b) octahedral crystal field environments.

distortion ($\delta > 0$), $g_\perp < g_\parallel \approx 2.0023$, while for negative distortion ($\delta < 0$) $g_\parallel < g_\perp < 2.0023$ and both *g* components are smaller than 2.0023, i.e., $g_\parallel < g_\perp < 2.0023$.

In an octahedral crystal field, T_{2g} is the ground state (Fig. 3b). Thus, the ground state will retain some orbital angular momentum even in zero order. The ESR signal is not observed for d^1 ions in purely octahedral symmetry. If the tetragonal distortion is positive, the d_{xy} orbital is the lowest and both *g* values are predicted to be less than 2.0023 ($0 < \delta \gg \lambda$ and $\Delta \gg \delta$). However, $g_\perp$ is smaller than $g_\parallel$.

Zr^{3+} in the silicalite structure (Zr-Sil) shows ESR spectra with $g_z < g_x$, $g_y < 2.0023$, or $g_\parallel < g_\perp < 2.0023$ and reveals a distorted tetrahedral geometry around Zr^{3+} and a $d_{x^2-y^2}$ orbital ground state. This means that zirconium with larger ionic radii (0.59 Å) cannot be accommodated in a perfect tetrahedral Si site which has an ionic radius of 0.26 Å and hence the local geometry distorts on incorporation of zirconium in the silicalite lattice and a defect center is formed. These results are consistent with the EXAFS data (N(Zr–O) = 3.81 and N(Zr–Si) = 1.21).

Active Sites in Selective Oxidation

It is well known that group IV–VI transition metals form peroxo/hydroperoxy species on interaction with aqueous hydrogen peroxide or organic hydroperoxides (ROOH; R = alkyl, aryl) (22). These peroxo- and/or hydroperoxo species have been proposed as intermediates or active centers in several oxidation reactions. In these reactions, the active metal site acts as a reducing agent and polarizes the dioxygen bond, facilitating the bond cleavage. It can also simultaneously bind dioxygen and the substrate and then create a favorable reaction pathway for selective oxidation.

When tetravalent metal ions such as Ti^{4+} and Zr^{4+} are incorporated in the silicalite framework, the resulting metallosilicalites are neutral in nature. The origin of the activity of these metallosilicalites in selective oxidation reactions using aqueous H_2O_2 is believed to be the stability of the corresponding metal–peroxo species (23). The active species and the reaction mechanism in the oxidation reactions have been proposed for Ti-containing molecular sieves, on the basis of ESR and EXAFS studies. In this case, five-membered cyclic hydrogen-bonded structure with a titanium hydroperoxo moiety, Ti–OOH, and a protic solvent molecule, e.g., water, was proposed as active species. It is evident from the structural investigations (*vide supra*) that Zr-silicalite samples contain isolated Zr^{4+} active centers, a prerequisite for the high H_2O_2 selectivity in comparison to the Zr-impregnated silicalite samples.

Studies on the catalytic activity of Zr-silicalite samples have already been reported (11, 12). Here, we have studied the behavior of isolated Zr active sites in the hydroxylation of phenol using different solvents. The results on the use of different solvents such as water, methanol, acetonitrile, and acetone under identical conditions in the hydroxylation of phenol on Zr-Sil-2 samples are summarized in Table 2. The solvents affect both the phenol conversion and H_2O_2 efficiency. Under identical conditions, the highest catalytic activity is obtained in the polar solvent, water. The sample showed 25.4% H_2O_2 selectivity with a turnover number (TON) (moles of phenol converted per mole of Zr atoms per hour) of 7.1. In contrast, negligible conversions were obtained in the solvents methanol and acetonitrile with a very low selectivity for the desired product, *viz*., hydroquinone (1.6 wt%). A significant selectivity for hydroquinone (11.4 wt%) was observed in acetone, but at a low conversion (TON = 0.3). This suggests an important role of a protic solvent, such as water, in this selective oxidation reaction. However, the similarity in the activity of acetonitrile and methanol, irrespective of their polarities, tempts us to conclude that the solvent effects on the catalytic activity are very intricate, being a function of polarity, molecular size, diffusion in the pores, and interaction of solvent molecules with active centers. The solvent might influence the stability of intermediates formed during the reaction and hence the activation of substrate molecule (24). The solvent molecules such as acetone and acetonitrile can interact and coordinate with isolated Zr^{4+} ions in the silicalite more effectively than H_2O (silicalite-1 and -2 are hydrophobic), increasing the four-fold coordination to a higher coordination around Zr^{4+} ions. Consequently, the formation of hydroperoxo species in the presence of H_2O_2, which is the active intermediate, is not much favored (24). Our ESR results lend support to this argument that the formation of the peroxide radical is indeed inhibited in the presence of other solvents such as acetonitrile and methanol (Fig. 4). The precise catalytic reaction mechanism associated with these isolated active zirconium centers is not yet understood, but the key events may be the interaction of H_2O_2 and a protic solvent, water, with the Zr active site and the transfer of a peroxide oxygen species to the phenol to be oxidized.

TABLE 2

Effect of Solvents in the Hydroxylation of Phenol[a]

Solvent	Dielectric constant (Debye, 298 K)	H_2O_2 sel[b]	Product distribution (wt%) PBQ	CAT	HQ	TON[c]
Water	81	25.4	1.3	41.9	44.6	7.1
Acetone	23	2.5	68.2	20.4	11.4	0.3
Acetonitrile	38	1.5	59.2	39.2	1.6	0.2
Methanol	33	1.0	63.5	34.9	1.6	0.1

[a] Reaction conditions: catalyst (Zr-Sil-2) = 0.5 g; solvent = 10 g; phenol/H_2O_2 (mol) = 3; reaction duration = 10 h; temperature = 353 K.

[b] H_2O_2 selectivity for the formation of *p*-benzoquinone (PBQ), catechol (CAT), and hydroquinone (HQ), excluding tar.

[c] TON = moles of phenol converted per mole of Zr atom per hour.

The catalytic properties of metallosilicalites are dependent on the nature and location of the metal ions in the framework, their accessibility to adsorbates, and their coordination with ligands. The spectroscopic features in the UV–visible as well as ESR spectra of hydroperoxide and superoxide species formed by framework Ti^{4+} in titanium silicalites in the presence of aqueous H_2O_2 have been well documented (25–27). A similar study on the formation of the superoxide radical ion on monoclinic zirconia has been reported by Giamello *et al.* (28). In the present study, the nature of the species formed during the interaction of Zr-Sil-1 and Zr-Sil-2 samples ($SiO_2/ZrO_2 = 102$) with H_2O_2 (50% aqueous) was investigated by ESR and UV–visible spectroscopic techniques.

ESR investigations revealed the formation of Zr(IV) superoxide ($Zr(O_2^{-\bullet})$) radical species. The spectra for Zr-Sil-1 and Zr-Sil-2 are only marginally different (g_z = 2.031, g_y = 2.009, and g_x = 2.003 for Zr-Sil-1 and g_z = 2.031, g_y = 2.010, and g_x = 2.004 for Zr-Sil-2; Table 3). A

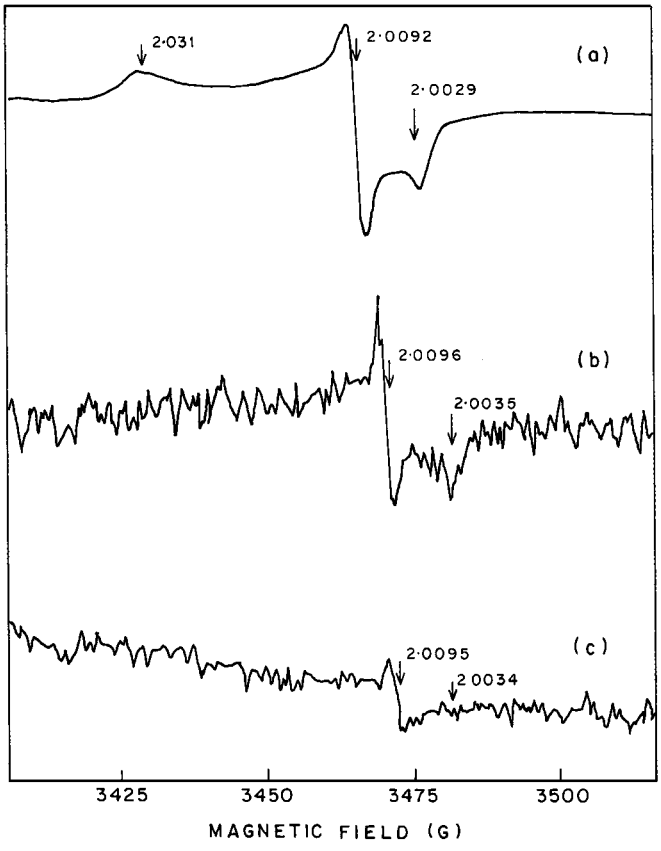

FIG. 4. Effect of (a) water, (b) acetonitrile, and (c) methanol on the ESR spectra of Zr(IV) superoxo radical species in Zr-Sil-1 formed after treatment with H_2O_2. The g parameters are marked.

representative spectrum for Zr-Sil-1 is depicted in Fig. 4a. The g values are close to those of the superoxide species formed on the surface of activated ZrO_2 ($g_z = 2.033$, $g_y = 2.010$, and $g_x = 2.003$) but differ especially in the g_z value for the superoxide ions associated with Ti^{4+} in TS-1 ($g_z = 2.027$, $g_y = 2.010$, and $g_x = 2.004$). The difference in g_z values of Zr- and Ti-containing silicalite samples is mainly attributed to the difference in the spin–orbit coupling parameters. A Zr-free silicalite sample did not show any ESR signal on interaction with H_2O_2. This gives evidence for the association of superoxide radical species with the zirconium ion. Interaction of Zr-Sil-2 samples with *tert*-butylhydroperoxide (TBHP), a bulkier oxidant, did not show any ESR signal, indicating the inaccessibility of Zr ions for the formation of any superoxide species with TBHP, and hence the presence of Zr inside the pore structure is supported. It is also evident that diffusion of the bulkier TBHP within the channels of the medium-pore Zr-silicalite samples is restricted. The ESR studies clarify that the superoxide species are formed only in the presence of Zr^{4+} ion inside the pore structure and that these isolated Zr^{4+} species are the active centers for the catalytic reactions.

TABLE 3

ESR Spin Hamiltonian Parameters of Zr^{3+} and Zirconium Superoxo Species in Silicalite Samples[a]

Sample	g_x	g_y	g_z
Zr^{3+} in Zr-Sil-1	1.982	1.973	1.968
Zr^{3+} in Zr-Sil-2	1.982	1.973	1.963
Zr^{3+} in Zr-impregnated Sil-2	1.977	1.977	1.958
Zr^{3+} in zirconia	1.978	1.978	1.953
$Zr(O_2^{-\bullet})$ species in Zr-Sil-1 exposed to water	2.003	2.009	2.031
$Zr(O_2^{-\bullet})$ species in Zr-Sil-2 exposed to water	2.005	2.010	2.031
$Zr(O_2^{-\bullet})$ species in Zr-Sil-1 exposed to acetonitrile	2.004	2.010	*b*
$Zr(O_2^{-\bullet})$ species in Zr-Sil-1 exposed to methanol	*b*	2.010	*b*
$Zr(O_2^{-\bullet})$ species in zirconia	2.003	2.010	2.034

[a] Estimated error in g values is ±0.001.
[b] Not visible due low signal-to-noise ratio.

In order to probe the role of solvent on the formation of the superoxide species, we initially exposed the samples to methanol and acetonitrile solvents and then interacted them with hydrogen peroxide. To our surprise, the signals of the superoxide radical species were very weak as shown in Figs. 4b and 4c. Unlike g_y, the g_x and g_z features are not quite obvious from the spectra. The weak spectra, hence, correspond only to traces of superoxide species in methanol- and acetonitrile-exposed Zr-Sil-1 samples. From the ESR spectra it can be concluded that the amount of $Zr(O_2^{-\bullet})$ species formed is solvent dependent. The concentration of the superoxide species was estimated from the ESR spectral intensity. In this study a known amount of the zirconium(IV) superoxide ion ($g_z = 2.034$, $g_y = 2.009$, $g_x = 2.003$) formed by the interaction of Zr propoxide (70 wt% solution in 1-propanol) with aqueous H_2O_2 was considered as the reference. The spectral area obtained by double integration reveals that the concentration of the superoxide species is an order of magnitude lower in CH_3CN and CH_3OH solvents than in H_2O and varies in the order $H_2O \gg CH_3CN > CH_3OH$. Interestingly, this trend follows the variation of TON in the phenol hydroxylation reaction (Table 2).

The diffuse reflectance spectra of Zr-Sil-2 treated with water and then with H_2O_2 were compared qualitatively. Zr-Sil-2 samples showed a characteristic ligand-to-metal charge transfer (CT) band ($O(p\pi) \rightarrow Zr(4d)$ orbitals) at 212 nm (11). Addition of water resulted in two new bands at 303 and 358 nm, in addition to the CT band. These new bands indicate a direct insertion of water ligands into the first coordination sphere of the Zr(IV) site that change tetrahedral coordination of Zr^{4+} to a higher coordination, mostly hexacoordinated. All these changes were completely reversible. Further addition of H_2O_2 gave rise to a spectrum which is characterized by a continuous broad absorption in the range of 250 to 400 nm, centered at

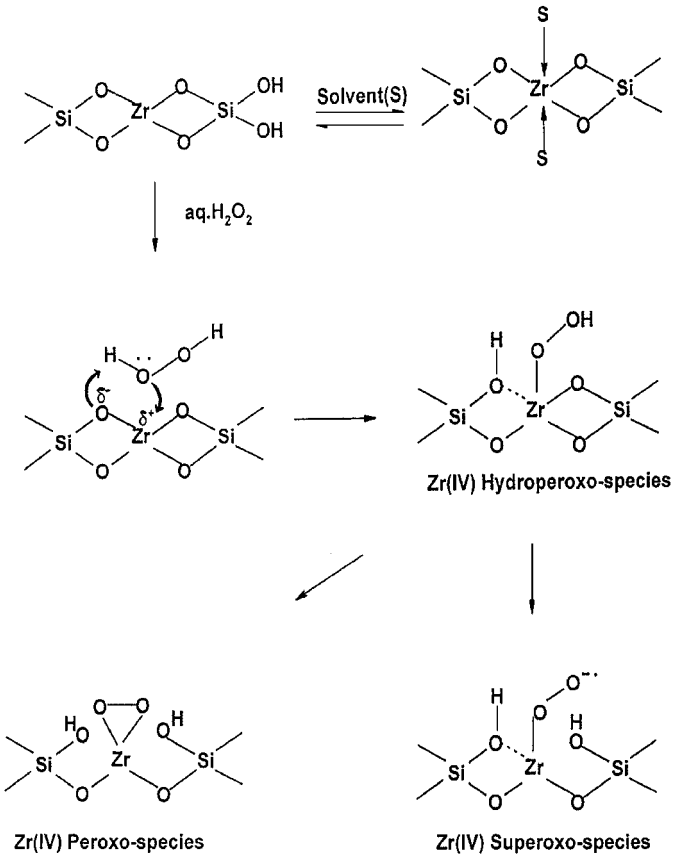

SCHEME 1

280 nm, along with the original CT band at 214 nm. This continuous absorption is associated with a charge transfer from a hydroperoxide species, which could not be detected in the ESR spectra due to its diamagnetic nature. This band disappeared on thermal treatment at 573 K for 1 h and only the CT band was observed.

Thus, the Zr^{4+} ions in the silicalite matrix are capable of coordinating to $O_2^{-\bullet}$ ions, formed in the presence of aqueous H_2O_2. Zr-Sil-1 and Zr-Sil-2 samples showed similar ESR and UV–visible spectra on interaction with solvents and H_2O_2. On the basis of the spectroscopic results and catalytic activity, we propose the mechanism shown in Scheme 1 for the interaction of Zr-Sil samples with aqueous H_2O_2.

CONCLUSIONS

The existence of Zr^{4+} in tetrahedral positions has been postulated on the basis of the XRD, FT-IR, and UV–visible data in our previous reports. From Zr-edge EXAFS spectral analysis, it is now established that Zr is in the tetrahedral coordination having Si–O–Zr linkages. Presumably an edge- and/or corner-sharing type of linkages connect the isolated ZrO_4 units to the silicalite framework. ESR studies of the reduced Zr-silicalite samples reveal a distorted tetrahedral geometry around Zr^{3+} and a $d_{x^2-y^2}$ orbital ground state, which is consistent with the above structures. The solvents have profound influence on the hydroxylation of phenol over Zr-silicalite samples. The formation of Zr(IV) superoxide radical species, as seen by ESR, is affected by the solvent molecules to different extents, in agreement with the variation of TON.

REFERENCES

1. Pei, S., Zajac, G. W., Kaduk, J. A., Faber, J., Boyanov, B. I., Duck, D., Fazzini, D., Morrison, T. I., and Yang, D. S., *Catal. Lett.* **21**, 333 (1993).
2. Bordiga, S., Boscherini, F., Coluccia, S., Genoni, F., Lamberti, C., Leofanti, G., Marchese, L., Petrini, G., Vlaic, G., and Zecchina, A., *Catal. Lett.* **26**, 195 (1994).
3. Bordiga, S., Coluccia, S., Lamberti, C., Marchese, L., Zecchina, A., Boscherini, F., Buffa, F., Genoni, F., Leofanti, G., Petrini, G., and Vlaic, G., *J. Phys. Chem.* **98**, 4125 (1994).
4. Cartier, C., Lortie, C., Trong On, D., Dexpert, H., and Bonneviot, L., *Physica.* **208/209,** 653 (1995).
5. Bittar, A., Adnot, A., Sayari, A., and Kaliaguine, S., Res. *Chem. Intermed.* **18**, 49 (1992).
6. Lamberti, C., Bordiga, S., Arduino, D., Zecchina, A., Geobaldo, F., Spanó, G., Genoni, F., Petrini, G., Carati, A., Villain, F., and Vlaic, G., *J. Phys. Chem. B* **102**, 6382 (1998).
7. Hatje, U., Hagelstein, M., Reßler, T., and Forster, H., *Physica* **208/209**, 646 (1995).
8. Bordiga, S., Buzzoni, R., Geobaldo, F., Lamberti, C., Giamello, E., Zecchina, A., Leofanti, G., Petrini, G., Tozzola, G., and Vlaic, G., *J. Catal.* **158**, 486 (1996).
9. Lamberti, C., Turnes-Palomino, G., Bordiga, S., Zecchina, A., Spano, G., and Otero-Arean, C., *Catal. Lett.* **63**, 213 (1999).
10. Prieto, C., Blasco, T., Camblor, M., and Perez-Pariente, J., *J. Mater. Chem.* **10**, 1383 (2000).
11. Rakshe, B., Ramaswamy, V., Vetrivel, R., and Ramaswamy, A. V., *Catal. Lett.* **45**, 41 (1997).
12. Rakshe, B., Ramaswamy, V., and Ramaswamy, A. V., *J. Catal.* **163**, 501 (1996).
13. Rakshe, B., and Ramaswamy, V., *Stud. Surf. Sci. Catal.* **113**, 219 (1998).
14. Rakshe, B., Ramaswamy, V., and Ramaswamy, A. V., *in* "Recent Trends in Catalysis" (V. Murugesan, B. Arabindo, and M. Palanichamy, Eds.), p. 529. Narosa Publishing House, New Delhi, India, 1999.
15. Vaarkamp, M., Linders, J. C., and Koningsberger, D. C., *Physica B* **159**, 208 (1995).
16. Ankudinov, A. L., and Rehr, J. J., *Phys. Rev. B* **56**, R1712 (1997).
17. Mieche-Brendle, J., Khouchaf, L., Baron, J., Le Dred, R., and Tuilier, M. H., *Microporous Mater.* **11**, 171 (1997).
18. Zecchina, A., Spotó, G., Bordiga, S., Ferrero, A., Petrini, G., Leofanti, G., and Padovan, M., *Stud. Surf. Sci. Catal.* **69**, 251 (1991).
19. Kustov, L. M., Zubkov, S. A., Kazansky, V. B., and Bondar, L. A., *Stud. Surf. Sci. Catal.* **69**, 303 (1991).
20. Prakash, A. M., and Kevan, L., *J. Catal.* **178**, 586 (1998).
21. Morterra, C., Giamello, E., Orio, L., and Volante, M., *J. Phys. Chem.* **94**, 3111 (1990).
22. Connor, J. A., and Ebsworth, E. A. V., *in* "Advances in Inorganic Chemistry and Radiochemistry" (H. J. Emeleus and A. G. Sharpe, Eds.), Vol. 6, p. 279. Academic Press, New York, 1964.

23. Bellusi, G., Carati, A., Clerici, M. G., Maddinelli, G., and Millini, R., *J. Catal.* **133**, 220 (1992).
24. Mal, N. K., and Ramaswamy, A. V., *J. Mol. Catal. A: Chemical* **105**, 149 (1996).
25. Geobaldo, F., Bordiga, S., Zecchina, A., Giamello, E., Leofanti, G., and Petrini, G., *Catal. Lett.* **16**, 109 (1992).
26. Tozzola, G., Mantegazza, A., Ranghino, G., Petrini, G., Bordiga, S., Ricchiardi, G., Lamberti, C., Zulian, R., and Zecchina, A., *J. Catal.* **179**, 64 (1998).
27. Bengoa, J. F., Gallegos, N. G., Marchetti, S. G., Alvarez, A. M., Cagnoli, M. V., and Yeramián, A. A., *Microporous Mesoporous Mater.* **24**, 163 (1998).
28. Giamello, E., Volante, M., Fubini, B., Geobaldo, F., and Morterra, C., *Mater. Chem. Phys.* **29**, 379 (1991).